

Computational Estimation of Chemical Reaction Rates in Extracellular Vesicle Signaling

Martin Damrath^a, Mohammad Zoofaghari^{b,c}, Milica Lekić^{a,d}, Hamid Khoshfekar Rudisari^{c,e}, Fabrizio Pappalardo^f, Mladen Veletić^{a,c}, Ilanko Balasingham^{a,c}

^aDepartment of Electronic Systems, Norwegian University of Science and Technology, Trondheim, Norway

^bDepartment of Electrical Engineering, Yazd University, Yazd, Iran

^cThe Intervention Centre, Oslo University Hospital, Oslo, Norway

^dFaculty of Electrical Engineering, University of Banja Luka, Banja Luka, Bosnia and Herzegovina

^eFaculty of Medicine, University of Oslo, Oslo, Norway

^fDepartment of Electrical, Electronic and Informatic Engineering, University of Catania, Catania, Italy

Abstract

The rates of chemical reactions involved in cell-to-cell communication can serve as a powerful tool for advanced theranostics and in establishing a molecular communication link between bio-transceivers. Reaction rates are usually experimentally measured by quantifying chemical products, which is challenging when several signal transduction mechanisms are involved in the signaling pathway. Without loss of generality, we focus on extracellular vesicle (EV) cell-to-cell signaling and propose a computational method to estimate the chemical reaction rates which characterize a process by which EVs are taken by cells. The method is based on measuring only the time-course of environmental EVs, and eliminates the need to measure either bound or internalized EVs which is usually essential for experimental evaluation of the rates by using advanced molecular imaging modalities. As an alternative to a proposed approximation by a linear system model, our computation exploits a nonlinear system model in which the impact of limited receptor sites on the recipient cell membrane is incorporated. The reaction rates are obtained through a suggested linear and iterative approach as well as a novel way of applying Michaelis-Menten kinetics in the frequency domain. The range of validity of each technique is evaluated by varying the number of free binding sites on the cell membrane in relation to the initial number of environmental EVs. In conclusion, the proposed methods are very effective in assessing the dynamics of the EV uptake using a simple *in vitro* platform.

Keywords: Extracellular vesicle, chemical reaction rates, computational biology, molecular communication.

1. Introduction

Extracellular vesicles (EVs) are nano-sized phospholipid spheres that are exchanged between cells in every living organism [1]. Cell-derived EVs act as signal transducers that can be used as diagnostic biomarkers and therapeutic agents [2]. The processes of EV release (e.g., exocytosis and vesicle budding) and uptake (e.g., endocytosis, fusion and phagocytosis), Figure 1, are characterized by chemical reaction rates which are studied in chemical kinetics [3, 4]. Values of chemical reactions involved in EV transport yield information about the reaction's mechanism and transition states, and are critical for the creation of mathematical models that are used as a tool to describe the characteristics of EV transport. Moreover, such values are essential for prototyping EV-based therapy [5, 6], for example, anticancer therapy [7], giving insights into how fast the biomolecule-carrying EV absorption occurs or what is the survival rate of cancer cells that is closely dependent on the rate and amount of the received biomolecules. Furthermore, values of chemical reactions are important for effectively establishing a communication link between bio-transceivers in an EV-based communication network [8, 9].

Reaction rates involved in the EV signaling pathway are usually measured experimentally where the characterization of

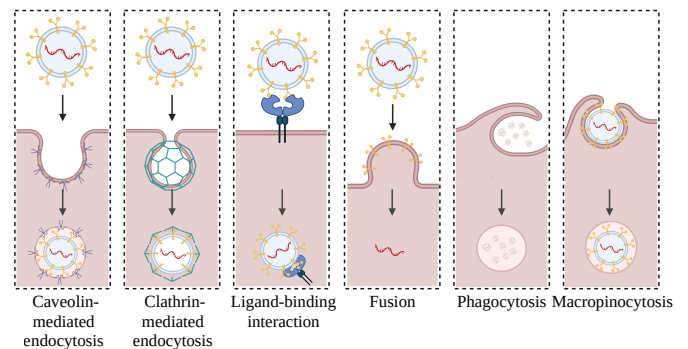


Figure 1: EV uptake by the recipient cell can be driven by many different pathways: endocytosis, fusion and juxtacrine. This illustration is created using BioRender.com.

EVs is done either by using techniques based on light scattering of particles, such as nanoparticle tracking analysis (NTA) and confocal microscopy (CM), or electron beam scattering of molecules, such as transmission electron microscopy (TEM) and scanning electron microscopy (SEM) [10]. NTA is used to evaluate the number and concentration of EVs, together with monitoring the dynamics of environmental EVs in the well after their isolation. Instead, TEM, CM and SEM are used to track

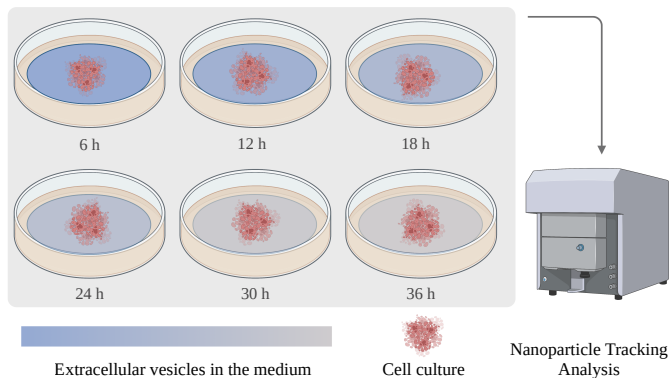


Figure 2: A schematic of experimental data acquisition for the suggested scenario of uptake rates estimation. This illustration is created using BioRender.com.

local interactions of EVs and the target cells. The current practice to measure the reaction rates associated with the uptake of EVs by cells is to monitor the time-course of the bound and internalized EVs and then determine the kinetic constants governing the interactions of EVs with the cell membrane. However, this strategy is not only technically challenging because it is hard to differentiate between the bound and internalized EVs when assaying acquired data [11], but also sensitive to potential mechanical deformations of the cell membrane incurred by its interaction with EVs [12].

Mathematical modeling is often used in combination with *in vitro* experiments to alleviate such limitations when deeply examining cell-to-cell signaling and identifying critical components involved in the signaling cascade [13]. Some examples where transport of (nano)particles were studied through mathematical models based on Fick’s second law of diffusion and a convection-diffusion-reaction equation, in combination with experimental models, include the stent-based drug release and delivery [14], the permeation of drugs through different layers of the skin [15], and the transport of a water-soluble drugs from cylindrical tablets [16]. Other examples include the models for tumor cell apoptosis upon drug reception [17] and nutrient uptake [18], as well as the models of the growth and invasion of Glioblastoma spheroids [19, 20].

We have recently proposed a computational approach which, in combination with a simple experimental setup, can be utilized for the estimation of chemical rates associated with the EV uptake [5]. In the experimental setup, the cells are cultured in multiple wells and then mixed with a known concentration of EVs, as illustrated in Figure 2. Different wells are used for different time-points of data acquisition where only the EVs present in the medium were quantified by NTA; in this regard, the time-course of the environmental EVs could be characterized. The suggested computational approach is based on a closed-form fitting function derived from ordinary differential equations (ODEs) that correspond to the kinetic model of EV uptake [5]. The suggested model, however, does not consider the number of available binding sites on the cell membrane which is a critical factor in the receptor-mediated endocytotic pathway of EV uptake.

Here we extend our previous model by exploiting a nonlinear system model in which the impact of limited receptor sites on the recipient cell membrane is incorporated. The reaction rates are then computed through a suggested iterative approach by which the rate parameters are obtained after several updates to satisfy the predefined relative error requirements. In the literature, several *time domain approaches* for parameter estimation have been well studied [21]. These techniques use a numerical method to iteratively solve the ODEs and estimate the parameters such that the norm of the object function is minimized. However, optimization algorithms often encounter convergence issues. For example, deterministic optimization methods are highly dependent on the initial estimation to avoid local minima, while stochastic optimization methods are time-consuming. Classical statistical estimators, such as the maximum likelihood method and the least square method, require large temporal data sets collected under different conditions, which are computationally intensive. Bayesian approaches require prior knowledge of parameters, which is usually obtained from preliminary experiments that increase the time and cost of the estimation process. To overcome these issues, we propose a *frequency domain approach* that results in closed-form expressions for the reaction rates. The closed-form expressions are used together with an iterative approach to simultaneously estimate the nonlinear part of the model and the rate parameters. This approach is also advantageous over existing methods, for example, an ill-posed inversion method [22] which is applicable for linear models and hardly satisfies the result uniqueness and stability.

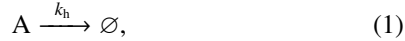
In addition, we extend our previous linear system model based solution in [5] by deriving closed-form expressions for rate estimation which avoids computationally complex curve fitting. Moreover, we suggest computing the reaction rates by applying Michaelis-Menten kinetics directly in the frequency domain under the pseudo-steady-state assumption. We compare the validity region of these three approaches with respect to the ratio between free receptor sites and environmental EVs, as well as the absolute values of the rate parameters. This is done by numerical particle-based simulations (PBS) which are set to resemble experimental data from the microscopic point of view, thus avoiding the time and resource-consuming experiments for the purpose of the presented results. Of note, our proposed methodology is not restricted to the estimation of the chemical reaction rates involved in EV signaling, and could be applied to analyses of reaction mechanisms and transition states involved in other types of molecular communication.

In the following, the considered system model for the current problem is presented in Section 2, and the iterative-, linear, and Michaelis-Menten approaches are defined in Section 3. Section 4 explains the PBS that is applied for evaluating the performance of the different approaches. The numerical results for selected parameter values extracted from the literature are discussed in Section 5, and the paper is concluded in Section 6.

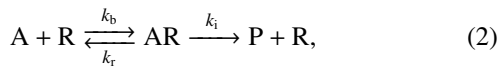
2. System Model

The Fick's law equation is exploited when constructing mathematical models of the spatio-temporal concentrations of particles which are governed by diffusion (including sub-diffusion in an anomalous media) and advection [16, 19, 20, 23]. Such models are typically referred to as partial-differential equation (PDE)-based models. On the other hand, ODE-based models are used to investigate the release and uptake rates of particles, as well as the dynamics of cell growth and death. In ODE-based models, the system model is characterized by a series of ODEs in which the unknowns are functions of time; in such models, coefficients characterizing diffusion and/or advection are excluded. Some examples where ODE-based models are utilized include studying the interactions between microglia and neural stem cells [24], the functionality of the immune system and normal cells in tumor growth [25], and the uptake of nutrients by a tumor cell with the presence of biomolecular fuel, such as glucose and lactate [18].

Here, we exploit an ODE-based system model to describe various mechanisms including fusion, receptor-mediated endocytosis, macropinocytosis and phagocytosis associated with EV uptake by cells [26] (Figure 1). EV fusion is accomplished by merging EVs with the cell membrane and releasing their content into the EV recipient cell cytoplasm. On the other hand, receptor-mediated pathways such as clathrin-mediated and caveolae-mediated endocytosis require a ligand on the EV membrane surface to employ specific receptors on the cell plasma membrane and leverage binding and internalization. We assume that the EV can be degraded in the environment via a first-order chemical reaction mechanism of the form



where 'A' indicates the unbound EVs and k_h is the degradation (half-life) chemical reaction rate. We also assume that the EV may reversibly react with a receptor 'R' to form an activated EV-receptor complex 'AR', via a second-order chemical reaction mechanism of the form



where k_b , k_r , and k_i are the binding-, recycling-, and internalization chemical reaction rate, respectively. Furthermore, 'P' denotes an EV finally internalized into the cell. Here we assume the number of the recipient cells is constant during the simulations and the chemical reaction rates are time-independent. Also, we assume that the uptake mechanism is not influenced by the number of initial EVs in the medium where the recipient cells are cultured [27].

Following (1) and (2), the dynamics of bound and environmental EVs are given by the following ODEs:

$$\frac{dq_{AR}(t)}{dt} = k_b f(t) - k_r q_{AR}(t) - k_i q_{AR}(t), \quad (3)$$

and

$$\frac{dq_A(t)}{dt} = -k_b f(t) + k_r q_{AR}(t) - k_h q_A(t), \quad (4)$$

respectively, satisfying the following initial conditions:

$$q_A(0) = Q_0, \quad q_{AR}(0) = 0. \quad (5)$$

The term $q_A(t)$ is the number of EVs in the environment (initially set to Q_0) and $q_{AR}(t)$ is the number of EVs bound to the cells.

We explore how limited receptor sites affect the dynamics of EVs using a function defined as

$$f(t) = [N - q_{AR}(t)] q_A(t), \quad (6)$$

where N is the total number of receptor sites per cell. When EVs are already bound to the receptors on the recipient cell membrane, the binding probability of the remaining EVs decreases. To account for this effect, we introduce a modification factor, given by $[N - q_{AR}(t)]$ in (6), which modifies the binding rate. This generates nonlinear terms in the equations for the binding of EVs to the cell membrane, namely (3) and (4). We discuss how to determine $f(t)$ using an iterative approach in Section 3.1.

3. Computational Approaches

We exploit a frequency domain approach to derive the closed-form expressions for the chemical rates estimation. This approach imposes low computational cost and provides a platform to characterize the binding, recycling and internalization rates simultaneously. The input data are supposed to be provided for the environmental EVs which are quantified by PBS when combining the approach with *in silico* modeling or NTA when combining the approach with *in vitro* modeling. Taking the Fourier transform of (3) and (4) yields

$$j\omega \tilde{Q}_{AR}(j\omega) = k_b \tilde{F}(j\omega) - k_r \tilde{Q}_{AR}(j\omega) - k_i \tilde{Q}_{AR}(j\omega), \quad (7)$$

and

$$j\omega \tilde{Q}_A(j\omega) = -k_b \tilde{F}(j\omega) + k_r \tilde{Q}_{AR}(j\omega) - k_h \tilde{Q}_A(j\omega) + Q_0, \quad (8)$$

respectively, where $\tilde{Q}_{AR}(j\omega)$, $\tilde{F}(j\omega)$ and $\tilde{Q}_A(j\omega)$ denote the Fourier transform of $q_{AR}(t)$, $f(t)$ and $q_A(t)$, respectively. A closed-form expression for $\tilde{Q}_{AR}(j\omega)$ is obtained from (7) in terms of $\tilde{F}(j\omega)$ as

$$\tilde{Q}_{AR}(j\omega) = \frac{k_b \tilde{F}(j\omega)}{j\omega + k_r + k_i}, \quad (9)$$

and a useful equation for the chemical rates estimation is derived from (8) as

$$H(j\omega) = \frac{\tilde{F}(j\omega)}{(j\omega + k_h) \tilde{Q}_A(j\omega) - Q_0} = -\frac{j\omega + k_r + k_i}{j\omega k_b + k_b k_i}. \quad (10)$$

We assume that k_h is known, as the half-life of EVs is a well-studied and easily investigated issue. In principle, k_h can also be estimated by reformulating (10), although this will increase the overall rate estimation error. Eq. (10) provides a way to extract closed-form expressions for the reaction rates, as we explain below. This advantage significantly reduces the estimation time,

unlike numerical methods in the time domain and statistical approaches. $H(j\omega)$ is a complex function that can be expressed in the following form

$$H(j\omega) = R(\omega) + jI(\omega), \quad (11)$$

where $R(\omega)$ and $I(\omega)$ denote the real and imaginary parts of $H(j\omega)$ given by

$$R(\omega) = -\frac{\omega^2 + k_r k_i + k_i^2}{k_b(\omega^2 + k_i^2)}, \quad (12)$$

and

$$I(\omega) = \frac{\omega k_r}{k_b(\omega^2 + k_i^2)}, \quad (13)$$

respectively. $I(\omega)$ has the peak value $I(\omega_p) = I_p$ at

$$\omega = \omega_p = k_i. \quad (14)$$

Two more expressions could be simply derived for k_b and k_r in terms of I_p given by

$$k_b = -\frac{k_r + k_i}{k_i R(0)}, \quad (15)$$

and

$$k_r = -\frac{2k_i I_p}{R(0) + 2I_p}, \quad (16)$$

respectively. Thus, we have closed-form solutions for the chemical reaction rates, which depend on only two points of $H(j\omega)$, the DC component and the maximum of the imaginary component. According to (10), we need to specify $\tilde{F}(j\omega)$ before estimating the rate parameters. This is discussed in the following subsection through an introduced iterative approach.

3.1. Iterative Approach

Here we propose an iterative approach to evaluate $\tilde{F}(j\omega)$. Given $\tilde{F}^{(i)}(j\omega)$ as the estimated function at the i^{th} iteration, $H^{(i)}(j\omega)$ can be expressed as

$$H^{(i)}(j\omega) = \frac{\tilde{F}^{(i)}(j\omega)}{(j\omega + k_h) \tilde{Q}_A(j\omega) - Q_0}, \quad (17)$$

where $\tilde{Q}_A(j\omega)$ and Q_0 are either measured by PBS or NTA, and $\tilde{F}^{(i)}(j\omega)$ is assumed to be known from the $(i-1)^{\text{th}}$ iteration. $H^{(i)}(j\omega)$ is updated at each iteration leading to the new estimated parameters i.e., $k_b^{(i)}$, $k_r^{(i)}$, $k_i^{(i)}$ given by (14)-(16). This approach is here referred to as the iterative closed-form (Iter. CF) approach, where the rate parameters are calculated by the closed-form expressions. The closed-form solution depends only on two points in the spectral signal and is thus quite sensitive to variations of them. Therefore, we propose a second method, termed iterative fitting (Iter. FIT), where we estimate the reaction rates by applying curve fitting to (17) instead of using the closed-form solution. Since the curve fitting is based on several samples, Iter. FIT is more robust against variations in the spectral signal. However, it encounters more computational costs and needs the initial guess of the reaction rates.

In both iterative approaches, $k_b^{(i)}$, $k_r^{(i)}$, and $k_i^{(i)}$ are used to calculate a new estimate $\tilde{F}^{(i+1)}(j\omega)$. In order to determine $\tilde{F}^{(i+1)}(j\omega)$, we combine (6) and (9) to derive an operator equation given by

$$q_A(t) = \left[\frac{\mathcal{I}}{N} + \mathcal{A}^{(i)} \right] \{ f^{(i+1)}(t) \}, \quad (18)$$

where $\mathcal{I}\{\cdot\}$ is the identity operator and $\mathcal{A}^{(i)}\{\cdot\}$ is given by

$$\mathcal{A}^{(i)}\{\cdot\} = \frac{q_A(t)}{N} \mathcal{F}^{-1} \left\{ \frac{k_b^{(i)}}{j\omega + k_r^{(i)} + k_i^{(i)}} \mathcal{F}\{\cdot\} \right\}. \quad (19)$$

The operators \mathcal{F} and \mathcal{F}^{-1} indicate the Fourier transform and the inverse Fourier transform, respectively.¹ Also, $f^{(i+1)}(t)$ denotes the estimated $f(t)$ at the $(i+1)^{\text{th}}$ iteration. We apply the estimated rate factors $k_b^{(i)}$, $k_r^{(i)}$, and $k_i^{(i)}$ in (19) and solve (18) using the gradient descent method (GDM) to find the updated value $f^{(i+1)}(t)$. At each iteration, we compare the relative errors of estimated rates with a predefined tolerance ϵ and make a decision about continuing or ending the iterative process. We assume the initial value $f^{(0)}(t)$ to be equal to $q_A(t)$. The flowchart for the proposed approach is illustrated in Figure 3.

However, the iterative process suffer from an accumulated estimation error by error propagation, especially for small values of N . Smaller values of N result in stronger nonlinearity and lower power of $f(t)$, as given by (6). Consequently, imprecise rate estimates will lead to a larger estimation error of $f^{(i+1)}(t)$. This yields inaccurate $H^{(i+1)}(j\omega)$ given by (17), which once again gets back to estimation of $f^{(i+2)}(t)$ through (18). We will compare the performance of Iter. CF and Iter. FIT in terms of N in Section 5.

3.2. Michaelis-Menten Approach

As we discussed in Section 3.1, convergence of the iterative approach towards precise rate estimates is challenging when the number of free sites on the target cells, N , is small compared to the environmental EVs. Thereby, we exploit an alternative approach based on *Michaelis-Menten* (MM) kinetics, which is one of the most commonly used models of enzyme kinetics, and discuss its performance through error analysis simulations. Based on the MM kinetics, we derive an equation for the rates estimation which exclude $\tilde{F}(j\omega)$ and is not significantly influenced by the noise. The determination of reaction rates based on MM kinetics typically requires a couple of measurements at different initial environmental EV concentrations. From the observation of the internalized EVs, the initial reaction rate is derived as a function of initial environmental EV concentrations. Finally, the reaction rates are obtained using a nonlinear regression of the results to MM equation. By using approximate Bayesian computation, the number of measurements can be reduced to the measurement at a single initial environmental EV concentration [28]. In contrast, the approach presented

¹Here, we use a calligraphic notation to indicate an operation on a function rather than a variable.

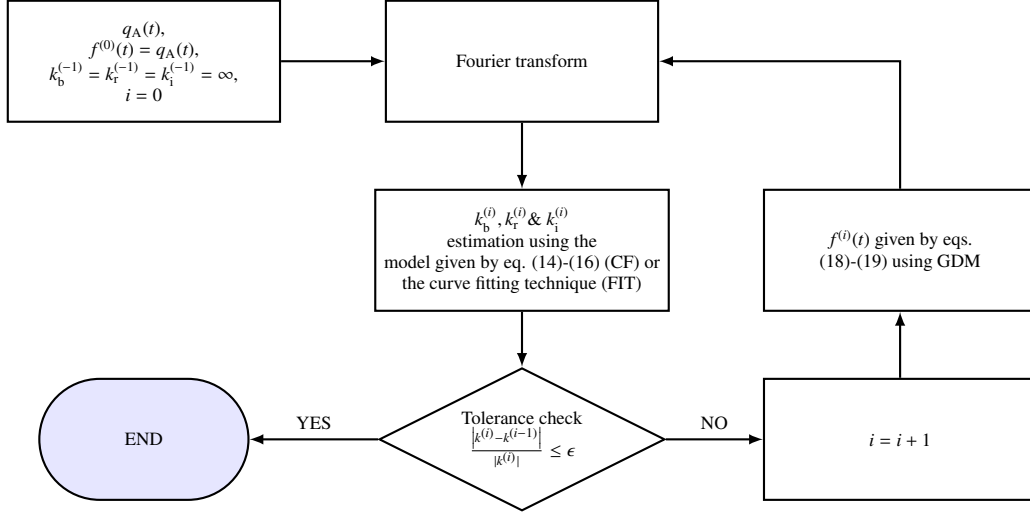


Figure 3: Flowchart of the iterative approach.

in the following exploits MM kinetics in the frequency domain and is based only on the temporal observation of environmental EVs at a single given initial concentration. Consequently, experimental determination of internalized EVs is not necessary in our approach.

The MM model is obtained under the quasi-steady-state assumption in which the concentration of bound EVs does not change in the time-scale of the internalization process. This condition is well-satisfied when the number of binding sites is small compared to the number of initial EVs. Mathematically, this means $\frac{\partial q_{AR}(t)}{\partial t} = 0$ and (3) is then transformed to

$$0 = k_b (N - q_{AR}(t)) q_A(t) - k_r q_{AR}(t) - k_i q_{AR}(t). \quad (20)$$

Replacing $q_{AR}(t)$ in (4) using (20) and solving the equation in the frequency domain, after some simple manipulations, yields

$$\begin{aligned} & ((j\omega + k_h) k_r + (j\omega + k_b N + k_h) k_i) \tilde{Q}_A(j\omega) + \\ & \left(\frac{j\omega k_b}{2} + k_b k_h \right) \tilde{Q}_s(j\omega) = \left(\frac{k_b Q_0}{2} + k_r + k_i \right) Q_0, \end{aligned} \quad (21)$$

where,

$$\tilde{Q}_s(j\omega) = \mathcal{F} \{ q_A(t) q_A(t) \}. \quad (22)$$

Eqs. (21) and (22) provide the new fitting equations for the rate estimations. Because this approach does not require approximating the nonlinear part of the model (i.e. $f(t)$) iteratively, it is computationally faster than the iterative approach. The performance of all presented approaches is compared in terms of N in Section 5.

3.3. Linear Model

When the number of receptor sites, N , is sufficiently large compared to the number of bound EVs, $q_{AR}(t)$ can be ignored in $f(t)$ given by (6), and the dynamics of $q_{AR}(t)$ and $q_A(t)$ are approximated by the following linear ODEs:

$$\frac{dq_{AR}(t)}{dt} \approx k_b N q_A(t) - k_r q_{AR}(t) - k_i q_{AR}(t), \quad (23)$$

$$\frac{dq_A(t)}{dt} \approx -k_b N q_A(t) + k_r q_{AR}(t) - k_h q_A(t). \quad (24)$$

In this way, $H(j\omega)$ in (10) is rewritten as

$$H(j\omega) = \frac{N \tilde{Q}_A(j\omega)}{Q_0 - (j\omega + k_h) \tilde{Q}_A(j\omega)}. \quad (25)$$

and the rate parameters are obtained using (14)-(16) accordingly. Please note that the iterative approach that addresses the estimation of $\tilde{F}(j\omega)$ is not relevant for the linear model.

4. Particle-based Simulation

To analyze the performance of the rate estimation methods presented in Section 3, we use numerical particle-based simulations, where a particle here is equivalent to an EV. PBS is a cost-effective and a more precise/high-resolution alternative to experiments, which are often expensive in terms of time and resources. PBS results resemble the experimental data from the microscopic point of view, in our case the interaction between EVs and the cell's receptors and their internalization. Due to the full control of the relevant parameters, PBS is well suited for parameter studies such as the one performed in Section 5. Besides the time and resource consuming effort, the direct control of all parameters as well as the determination of reference parameters in experiments is crucial. In contrast to the ODE solution according to (3) and (4) which describes the mean expected behavior, in PBS the reaction statistics are applied to each particle. Thus, randomness is introduced and an individual result is obtained for each realization, which deviates from the ODE solution. We denote the deviation of the PBS results from the ODE solution as noise.

We focus our PBS on the degradation and uptake mechanism given in (1) and (2). In this context, we assume that a total of N receptor sites are available in the environment to interact with EVs. These receptor sites can be either from a single cell

or from multiple cells. Furthermore, we assume that all environmental EVs are subject to the same reaction rates and are present within the range of the receptor sites all the time and thus are available for interaction. By this assumption we can neglect the spatial component and focus on the reactions according to (1) and (2). Depending on whether an EV is in the environment or bound to a receptor site, it can react via two (pseudo) first-order pathways. Based on the reaction rates, we can determine probabilities for the reaction of an EV within a time interval Δt [29]:

$$p_h = \frac{k_h}{k_h + k_{b^*}} \left(1 - e^{-\Delta t(k_h + k_{b^*})}\right), \quad (26)$$

$$p_b = \frac{k_{b^*}}{k_h + k_{b^*}} \left(1 - e^{-\Delta t(k_h + k_{b^*})}\right), \quad (27)$$

$$p_r = \frac{k_r}{k_r + k_i} \left(1 - e^{-\Delta t(k_r + k_i)}\right), \quad (28)$$

$$p_i = \frac{k_i}{k_r + k_i} \left(1 - e^{-\Delta t(k_r + k_i)}\right), \quad (29)$$

$$k_{b^*} = k_b (N - q_{AR}(t)), \quad (30)$$

where p_h , p_b , p_r , p_i are the degradation (half-life), effective binding, recycling, and internalization probabilities of an EV, respectively. Furthermore, k_{b^*} denotes the effective binding rate, which depends on the binding rate and on the number of free receptor sites. It allows us to interpret the binding reaction of an EV as a pseudo first order reaction. In PBS, for discrete time steps of length Δt for each EV, the probability of the possible chemical reactions is evaluated by a Bernoulli random variable where the probability of success is equal to the probability of reaction. If a reaction occurs, the number of environmental and/or bound EVs, as well as the number of free receptor sites, is adjusted for the next discrete time step.

5. Numerical Results

In this section, we investigate the validity of the approaches presented in Section 3 and their estimation errors by numerical particle-based simulations colorblackdiscussed in Section 4. The curve fitting for non-negative parameter estimation in the Iter. FIT and MM approaches is performed by the `MATLAB Optimization ToolboxTM`, which uses a trust-region-reflective method [30]. For our considered parameters discussed in Section 5.1, the initial guesses of the curve fitting algorithm applied in the Iter. FIT and MM approaches are chosen to be 10^0 for k_i and 10^{-1} for k_b and k_r . These are not to be confused with the initialized rates $k_b^{(-1)} = k_r^{(-1)} = k_i^{(-1)}$ for the initial tolerance check in Figure 3. All rates in the curve fitting algorithm are upper bounded by 10. When performing curve fitting, we do not consider the entire spectral signal, but only the region in which 97% of the spectral energy of $\hat{Q}_A(j\omega)$ in MM or of the denominator of $H(j\omega)$ in Iter. FIT lies (typically at low frequencies). The Iter. CF and linear approach depend only on the DC part and the maximum of the imaginary part of $H(j\omega)$ whose angular frequency is equal to the internalization rate (see (14)). By observing $q_A(t)$, we can roughly estimate the order of magnitude of k_i . Therefore,

Table 1: Default simulation parameters, which are applied throughout the numerical results, if not stated otherwise. Parameters with a bar denote dimensional parameters.

Parameters	Symbol	Value	Ref.
Binding rate	k_b	0.13	[31]
Recycling rate	k_r	0.11	[32]
Internalization rate	k_i \bar{k}_i	1 0.0046 s ⁻¹	[31]
Half-life rate	k_h	0	[31]
Binding sites	N	0.1 (MM) 1 (Iter. FIT) 10 (Iter. CF) 10 (Lin.)	
Initial EV quantity	Q_0 \bar{Q}_0	1 10 ⁵	[31]
Samples in PBS	N_s	10 ⁵	
PBS Monte Carlo runs	N_{MC}	10 ³	
Tolerance	ϵ	10 ⁻³	

we generously restrict the considered frequency range for these two approaches in our scenario to $|\omega| < 10$. By this procedures we prevent a large influence of low energy signal components on the curve fitting and numerical edge effects.

In order to evaluate the performance of the different proposed approaches, we utilize the normalized mean squared estimation error (NMSEE) which is defined as

$$\overline{\text{NMSEE}} = \frac{1}{N_{MC}} \sum_{n=0}^{N_{MC}-1} \left| \frac{k - \hat{k}}{k} \right|^2, \quad (31)$$

where N_{MC} is the number of PBS realizations and \hat{k} is the estimated rate.

5.1. Parameter Selection

The simulation parameters and rate parameters under consideration are given in Table 1. We use the listed parameters as reference parameters, which are assumed for the numerical simulations if the parameter is not varied. Inspired by [31], we consider a dimensionless scenario which is more general and compact since units are omitted. To achieve this, all concentrations are given relative to the initial environmental EV concentration \bar{Q}_0 and all temporal parameters are given relative to \bar{k}_i . Accordingly, the dimensionless parameters can be determined as

$$Q_0 = \frac{\bar{Q}_0}{\bar{Q}_0}, \quad N = \frac{\bar{N}}{\bar{Q}_0}, \quad k_b = \frac{\bar{k}_b \bar{Q}_0}{\bar{k}_i}, \quad k_{h,r,i} = \frac{\bar{k}_{h,r,i}}{\bar{k}_i}, \quad t = \bar{k}_i \bar{t}. \quad (32)$$

In [31], \bar{k}_b is given in units of mL/molecule/s and the reactant in molecule/mL. In PBS, we work with the absolute number of EVs and receptor sites, which needs to be taken into account in the calculation of the dimensionless binding rate k_b . However,

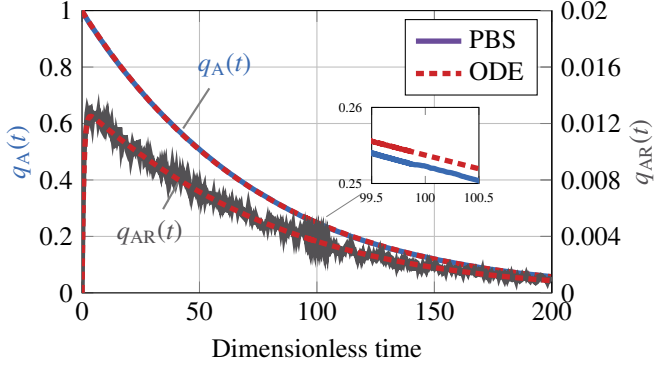


Figure 4: Obtained number of EVs in environment and bound to the cell with respect to time for a single PBS realization and ODE solution of (3) and (4). The considered parameters are given in Table 1 and $N = 0.1$.

this is not important for the evaluation of our estimation methods and we therefore omit the calculation and directly adopt the dimensionless parameter from [31] for the sake of simplicity. The variation of individual parameters can influence the total time until all environmental EVs are internalized and thus the temporal dynamics. To counteract this effect and capture the full dynamics of the signal, we consider in the simulations the period adaptive between zero and ten times the duration that is theoretically needed to internalize 90% of all EVs based on (3) and (4). We divide this range into N_s equally distributed samples. As an example, for the scenario in Figure 4 this results in a total time of $10 \times 163 = 1630$ with a step size of $\Delta t = 0.0163$. It should be noted that in PBS N_s is limited only by hardware, whereas in laboratory measurements the sampling rate is determined by the available equipment and the temporal effort. A sufficient required time resolution of the laboratory measurements can nevertheless be achieved by interpolation between and/or extrapolating beyond the measuring points.

Figure 4 shows $q_A(t)$ and $q_{AR}(t)$ for a single realization of the PBS. As a comparison, the ODEs (3) and (4) are numerically solved as well. It can be observed that the noisy PBS simulation follows the ODE solution.

5.2. Parameter Studies

In the following, we examine the performance of the rate estimation approaches introduced in Section 3 with respect to the parameters. Figure 5 shows the performance of the four different approaches with varying number of binding sites N . It should be mentioned that N represents the ratio of binding sites to initial environmental EVs. This can be achieved experimentally by changing the number of binding sites \bar{N} , for example, by varying the number or type of cells. On the other hand, the initial environmental EV concentration \bar{Q}_0 can be increased or decreased. From Figure 5, different regions can be identified where each approach is preferable and provides useful rate estimates. Depending on N , all approaches have their justification. For better visualization, we have highlighted three regions in color and labeled them with the approaches that give an $\text{NMSEE} < 10^0$ at all three rate estimates. The MM approach

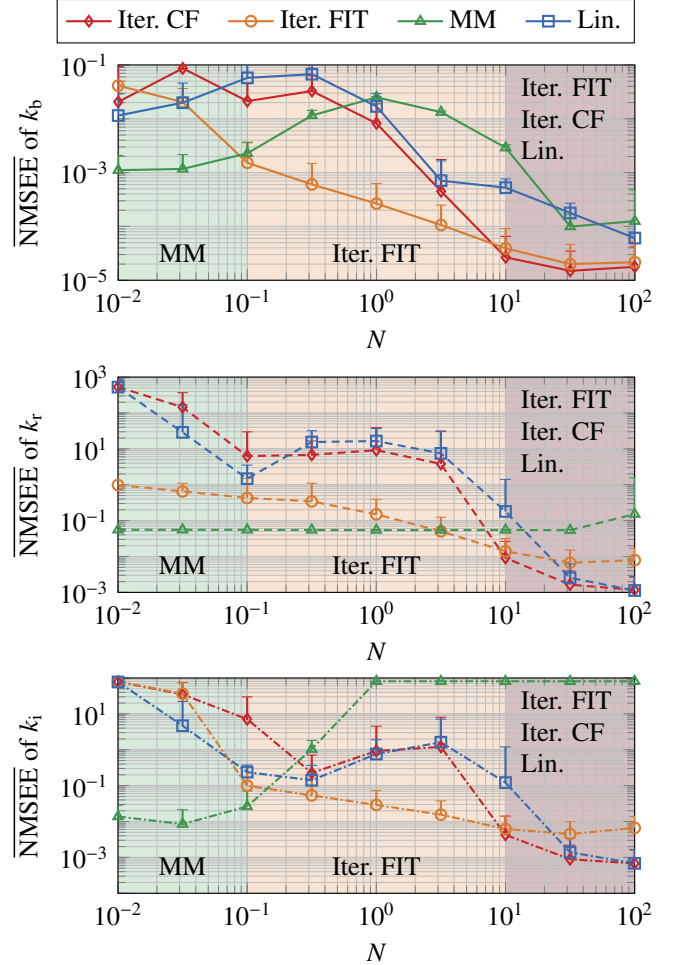


Figure 5: Normalized mean squared estimation error for the reaction rates with respect to number of binding sites of the cells. The considered parameters are given in Table 1.

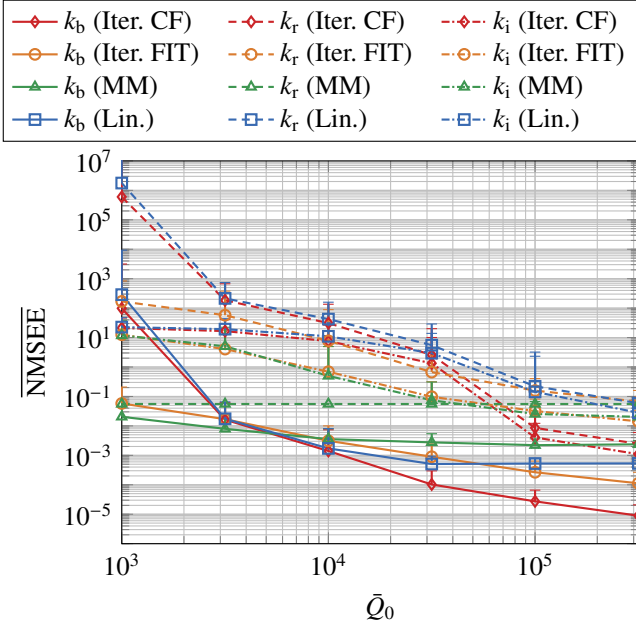


Figure 6: Normalized mean squared estimation error for the reaction rates with respect to initial EV quantity in the medium. The considered parameters are given in Table 1. Since N is fixed, the dimensional number of binding sites changes accordingly.

performs best in the region with low N . In this region, the governing MM kinetics assumption that the substrate concentration is much larger than the enzyme concentration is fulfilled and the quasi-steady-state assumption is satisfied. The maximum of the MM approach observed for k_b and $N = 10^0$ is due to the upper bound of all rates in the curve fitting algorithm. From $N = 10^0$ the estimate of k_i reaches this upper bound, which is compensated by a decreasing NMSEE for k_b as N increases. A low N also means a more dominant nonlinear part in (6). This leads to poor performance of both the iterative approach and the linear approach. Conversely, the influence of the nonlinear part in (6) decreases as N increases. This improves the rate estimation of the iterative approach as well as the rate estimation of the linear approach, which is based only on the linear part in (6). The iterative approach provides the best rate estimates for the parameters under consideration especially in the range $10^{-1} < N < 10^2$. Iter. FIT outperforms Iter. CF clearly for $N < 10^1$. In this range the spectral signal becomes more noisy. While the closed-form solution depends only on two points in the spectral signal and is therefore sensitive to noise, curve fitting based on numerous points offers more robustness against noise. Furthermore, it can be concluded from Figure 5 that, for the assumed scenario, the estimation of k_b is more accurate than the estimation of k_r and k_i .

In the remaining analysis, we investigate the influence of individual system parameters on the performance of the rate estimation approaches. In doing so, we set N for each individual approach to a value where the respective approach performs well, as listed in Table 1. Figure 6 shows the influence of the initial number of environmental EVs, \bar{Q}_0 , on the NMSEE when estimating k_b , k_r and k_i . Since N is fixed, \bar{N} changes accord-

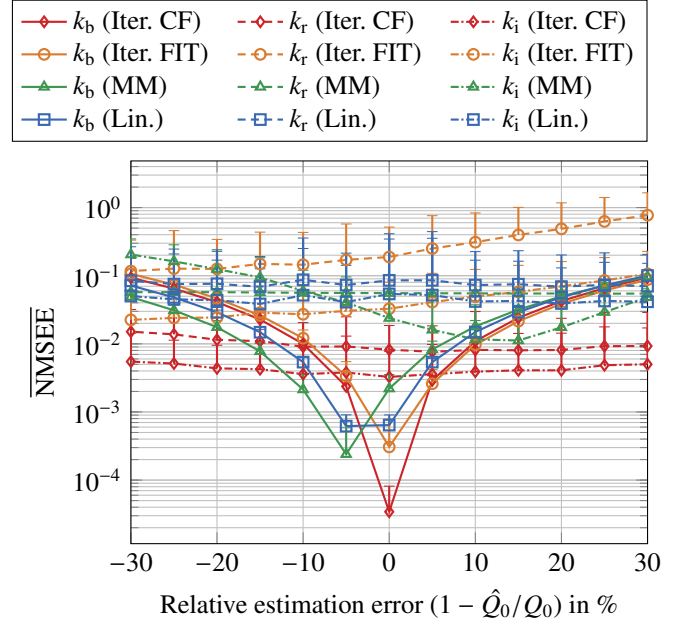


Figure 7: Normalized mean squared estimation error for the overestimation (negative relative estimation error) and underestimation (positive relative estimation error) of the initial EV quantity in the well. The considered parameters are given in Table 1.

ingly. For all rates, the estimation improves with increasing \bar{Q}_0 . This is to be expected, since the deviation from the expected value decreases with increasing number of EVs in PBS. In other words, the PBS result approaches the solution given in (3) and (4) as \bar{Q}_0 increases. For the scenario under investigation, at least $\bar{Q}_0 = 10^4$ EVs for MM approach, at least $\bar{Q}_0 = 10^{4.5}$ EVs for Iter. FIT, and at least $\bar{Q}_0 = 10^5$ EVs for Iter. CF and linear approach should be selected to bring the NMSEE of all rates below 10^0 .

Our proposed rate estimation approaches require knowledge of N and Q_0 . While Q_0 is comparatively easy to measure directly, \bar{N} can be determined by additional saturation binding assay experiments and estimated for the final experiment. However, both are experimentally determined values that involve a certain degree of imprecision. Figure 7 illustrates this influence on the rate estimate when Q_0 is overestimated or underestimated indicated by \hat{Q}_0 . Note that Q_0 is dimensionless and N is given relative to it. Thus, an overestimation of Q_0 can also be interpreted as an underestimation of N , and an underestimation of Q_0 as an overestimation of N as well. Figure 7 shows that over- or underestimation mainly affects the NMSEE of k_b . This observation is consistent with previous analysis [5]. The reason is that the binding process described by k_b is directly influenced by Q_0 , while k_r and k_i depend only on the bound EVs. For the assumed scenario, the NMSEE is below 10^0 for all rate estimates even with an over- or underestimation of Q_0 up to 30%. This result demonstrates that the proposed approaches are robust to an imprecise determination of Q_0 and N .

Besides the determination of Q_0 and N , the experimental measurement of $q_A(t)$ will also be subject to measurement noise. Reasons for this are, for example, variations of envi-

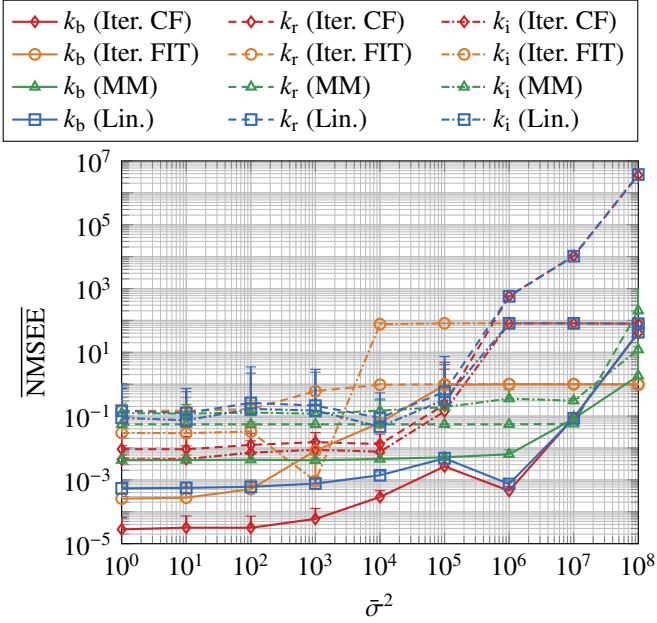


Figure 8: Normalized mean squared estimation error for the reaction rates with respect to additive white Gaussian noise variance. The considered parameters are given in Table 1.

ronmental parameters like temperature or imperfection of the used measuring instruments. To investigate the influence of these macroscopic noise sources on the rate estimation, we add a zero-mean additive white Gaussian noise with a variance of $\bar{\sigma}^2$ to the PBS samples. Please note that $\bar{\sigma}^2$ is given in dimensional form. Figure 8 shows the impact of different $\bar{\sigma}^2$ values on the performance of each approach. As expected, the performance of all rate estimation approaches decreases as the noise power increases. However, noise affects the different estimates differently. The multiplication $j\omega\hat{Q}_A(j\omega)$ in the MM and Iter. FIT approach leads to an increased noise power with increasing frequency. Increasing $\bar{\sigma}^2$ leads to a wider considered frequency range in which 97% of the energy lies. The noise samples falling into the extended frequency range thus degrade the rate estimation using curve fitting. In contrast, Iter. CF and the linear approach are based on closed-form expressions and the relevant frequency range is fixed. The noise here is mainly manifested by a noisy spectral signal, which with increasing $\bar{\sigma}^2$ affects the amplitude values and the location of the maximum in the imaginary part of $H(j\omega)$, which are essential for this estimation approach. As can be seen from Figure 8, the MM approach shows the highest robustness to the added measurement noise, whereas the Iter. FIT approach is the most vulnerable.

Figure 9 shows the effect on the NMSEE of k_b , k_r , or k_i when these are varied over a wide range, respectively. For the MM approach, it is noteworthy that the NMSEEs for k_b and k_r have a clear minimum at 10^{-1} . This can be explained by the fact that the initial point of the curve fitting algorithm for these rates is chosen exactly at 10^{-1} . While the MM approach gives poor estimates at low rates for the scenario under investigation, the other three approaches show a more robust behavior, at least for k_b and k_i . Both rates provide an NMSEE of less than 10^0 for the

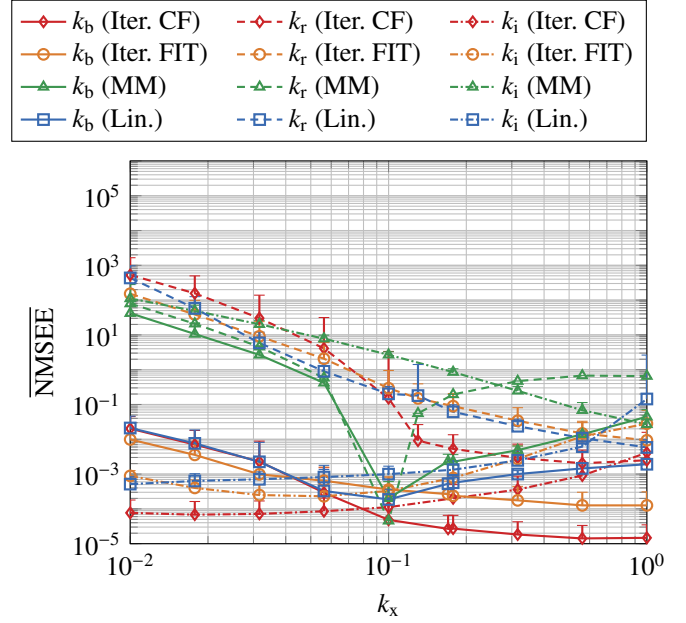


Figure 9: Normalized mean squared estimation error for the reaction rates with respect to reaction rate value. The considered parameters are given in Table 1.

considered scenario. Only k_i shows a higher NMSEE for $k_i < 10^{-1}$. The results demonstrate that the proposed approaches are strongly dependent on the chosen parameters. Especially due to the nonlinearity in the system, certain parameter combinations can lead to high estimation errors. Likewise, increasing either \hat{Q}_0 (less noise in the PBS), N_s (wider frequency range) or the total observation time (higher frequency resolution) can lead to an improvement of the rate estimates.

5.3. Computational Complexity Analysis

In the following, a comparison of the computational complexity of the proposed approaches is given. Among all considered approaches, the curve fitting algorithm is the one with the highest computational complexity, followed by the gradient descent method and the calculation of the closed-form expressions. Consequently, the linear approach has the least computational complexity. If Iter. CF requires multiple iterations, its computational complexity is higher than that of a single curve fitting call in the MM approach. One iteration of the Iter. FIT approach is significantly more complex than an Iter. CF iteration. The number of iterations depends strongly on the chosen error tolerance ϵ , as well as on the general scenario. For the scenario under investigation and the parameter study from Figure 5, the average number of required iterations of the iterative approaches are shown in Figure 10. It can be seen that a maximum of 10 and 16 iterations on average are required for the Iter. CF and Iter. FIT, respectively. It can also be observed that the number of required iterations decreases for small and large values of N , and is generally similar for both approaches.

6. Conclusion

We designed original computational methods for the estima-

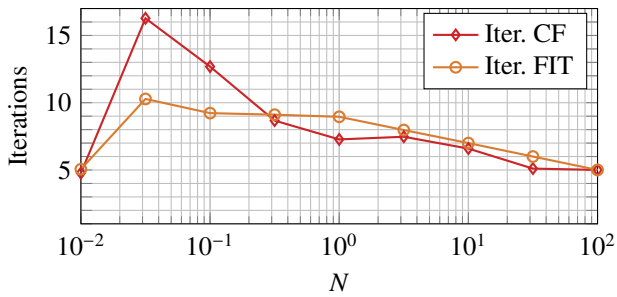


Figure 10: The average number of required iterations of the iterative approach with respect to number of binding sites of the cells. The considered parameters are given in Table 1.

tion of chemical reaction rates involved in the EV signaling pathway, particularly associated with the process of EV uptake by recipient cells. They are meant to be combined with a simple experiment, where the recipient cells are cultured in a well and mixed with the known number/concentration of the EVs, from which data are acquired. Our proposed approaches exploit only the monitored number of EVs in the medium where the cells are cultured, without any need to monitor the EVs that either bound to- or internalize into the recipient cells. For the purpose of demonstrating the validity of our approaches, we used particle-based simulations for generating synthetic data that resemble experimental data, thus omitting to conduct actual experiments. The performance of the proposed methods is evaluated and thoroughly discussed using the normalized mean squared estimation error. We managed to obtain the normalized mean squared estimation error for the EV binding rate of less than 10%, even with an overestimation or underestimation of the number of initial EVs up to 30%; this is the highest precision among the estimated rates. Future work will consist in combining our model with real data to identify adequate mathematical models of EV signaling more finely. This will largely help the development of EV-mediated therapy and EV-mediated molecular communication links.

Acknowledgment

This work was funded in part by the Research Council of Norway under the grant #287112 (CIRCLE – Communication Theoretical Foundation of Wireless Nanonetworks), the EU-H2020-FETOpen under the grant #828837 (GLADIATOR – Next-generation Theranostics of Brain Pathologies with Autonomous Externally Controllable Nanonetworks: a Trans-disciplinary Approach with Bio-nanodevice Interfaces), and the University of Catania (Application of Theoretical Telecommunication Models as a Novel Approach for the Study of Cell-to-Cell Communication Mediated by Exosomes in the Context of Neurodegenerative Diseases).

References

[1] G. Raposo, P. D. Stahl, Extracellular vesicles: a new communication paradigm?, *Nature Reviews Molecular Cell Biology* 20 (9) (2019) 509–510.

[2] H. Arjmandi, H. K. Rudsari, J. Santos, M. Zoofaghari, O. Ievglevskiy, M. Kanada, A. Khaleghi, I. Balasingham, M. Veletić, Extracellular vesicle-mediated communication nanonetworks: Opportunities and challenges, *IEEE Communications Magazine* 59 (5) (2021) 68–73. doi:10.1109/MCOM.001.2000994.

[3] S. Ferguson, R. Weissleder, Modeling EV kinetics for use in early cancer detection, *Advanced biosystems* 4 (12) (2020) 1900305.

[4] E. Bonsergent, E. Grisard, J. Buchrieser, O. Schwartz, C. Théry, G. Lavieu, Quantitative characterization of extracellular vesicle uptake and content delivery within mammalian cells, *Nature communications* 12 (1) (2021) 1–11.

[5] M. Zoofaghari, M. Damrath, H. K. Rudsari, F. Pappalardo, M. Veletić, I. Balasingham, Reaction rates estimation for the endocytic reception in extracellular vesicles-mediated communications, in: *Proceedings of the 9th ACM International Conference on Nanoscale Computing and Communication, NANOCOM '22*, Association for Computing Machinery, New York, NY, USA, 2022, p. 1–6. doi:10.1145/3558583.3558848.

[6] L.-G. Wu, Kinetic regulation of vesicle endocytosis at synapses, *Trends in neurosciences* 27 (9) (2004) 548–554.

[7] Y. Gao, Y. Qin, C. Wan, Y. Sun, J. Meng, J. Huang, Y. Hu, H. Jin, K. Yang, Small extracellular vesicles: a novel avenue for cancer management, *Frontiers in Oncology* 11 (2021) 638357.

[8] M. Veletić, M. T. Barros, I. Balasingham, S. Balasubramaniam, A molecular communication model of exosome-mediated brain drug delivery, in: *Proceedings of the Sixth Annual ACM International Conference on Nanoscale Computing and Communication, NANOCOM '19*, Association for Computing Machinery, New York, NY, USA, 2019, p. 1–7. doi:10.1145/3345312.3345478.

[9] H. K. Rudsari, M. Zoofaghari, M. Veletić, J. Bergsland, I. Balasingham, The end-to-end molecular communication model of extracellular vesicle-based drug delivery, *IEEE Transactions on NanoBioscience* (2022). doi:10.1109/TNB.2022.3206908.

[10] H. Shao, H. Im, C. M. Castro, X. Breakefield, R. Weissleder, H. Lee, New technologies for analysis of extracellular vesicles, *Chemical reviews* 118 (4) (2018) 1917–1950.

[11] I. Prada, J. Meldolesi, Binding and fusion of extracellular vesicles to the plasma membrane of their cell targets, *International journal of molecular sciences* 17 (8) (2016) 1296.

[12] Y. Guan, X. Shan, F. Zhang, S. Wang, H.-Y. Chen, N. Tao, Kinetics of small molecule interactions with membrane proteins in single cells measured with mechanical amplification, *Science Advances* 1 (9) (2015) e1500633.

[13] M. K. Domanska, V. Kiessling, A. Stein, D. Fasshauer, L. K. Tamm, Single vesicle millisecond fusion kinetics reveals number of snare complexes optimal for fast snare-mediated membrane fusion., *The Journal of Biological Chemistry* 285 (15) (2010) 11753.

[14] C. M. McKittrick, S. McKee, S. Kennedy, K. Oldroyd, M. Wheel, G. Pontrelli, S. Dixon, S. McGinty, C. McCormick, Combining mathematical modelling with in vitro experiments to predict in vivo drug-eluting stent performance, *Journal of Controlled Release* 303 (2019) 151–161.

[15] S. Hansen, A. Henning, A. Naegel, M. Heisig, G. Wittum, D. Neumann, K.-H. Kostka, J. Zbytovska, C.-M. Lehr, U. F. Schaefer, In-silico model of skin penetration based on experimentally determined input parameters. part i: Experimental determination of partition and diffusion coefficients, *European Journal of Pharmaceutics and Biopharmaceutics* 68 (2) (2008) 352–367.

[16] N. Wu, L.-S. Wang, D. C.-W. Tan, S. M. Moochhala, Y.-Y. Yang, Mathematical modeling and in vitro study of controlled drug release via a highly swellable and dissoluble polymer matrix: polyethylene oxide with high molecular weights, *Journal of controlled release* 102 (3) (2005) 569–581.

[17] M. A. Alqudah, Cancer treatment by stem cells and chemotherapy as a mathematical model with numerical simulations, *Alexandria Engineering Journal* 59 (4) (2020) 1953–1957.

[18] B. Mendoza-Juez, A. Martínez-González, G. F. Calvo, V. M. Pérez-García, A mathematical model for the glucose-lactate metabolism of in vitro cancer cells, *Bulletin of mathematical biology* 74 (5) (2012) 1125–1142.

[19] E. Luján, L. N. Guerra, A. Soba, N. Visacovsky, D. Gandía, J. C. Calvo, C. Suárez, Mathematical modelling of microtumour infiltration based on in vitro experiments, *Integrative Biology* 8 (8) (2016) 879–885.

[20] A. M. Stein, T. Demuth, D. Mobley, M. Berens, L. M. Sander, A

mathematical model of glioblastoma tumor spheroid invasion in a three-dimensional in vitro experiment, *Biophysical journal* 92 (1) (2007) 356–365.

- [21] P. Loskot, K. Atitey, L. Mihaylova, Comprehensive review of models and methods for inferences in bio-chemical reaction networks, *Frontiers in genetics* (2019) 549.
- [22] A. Mhamdi, W. Marquardt, An inversion approach to the estimation of reaction rates in chemical reactors, in: 1999 European Control Conference (ECC), IEEE, 1999, pp. 3041–3046.
- [23] A. Naegel, S. Hansen, D. Neumann, C.-M. Lehr, U. F. Schaefer, G. Wittum, M. Heisig, In-silico model of skin penetration based on experimentally determined input parameters. part ii: Mathematical modelling of in-vitro diffusion experiments. identification of critical input parameters, *European journal of pharmaceutics and biopharmaceutics* 68 (2) (2008) 368–379.
- [24] A. J. Alqarni, A. S. Rambely, I. Hashim, Dynamic modelling of interactions between microglia and endogenous neural stem cells in the brain during a stroke, *Mathematics* 8 (1) (2020) 132.
- [25] S. A. Alharbi, A. S. Rambely, A new ode-based model for tumor cells and immune system competition, *Mathematics* 8 (8) (2020) 1285.
- [26] K. J. McKelvey, K. L. Powell, A. W. Ashton, J. M. Morris, S. A. McCracken, Exosomes: mechanisms of uptake, *Journal of circulating biomarkers* 4 (2015) 7.
- [27] C. A. Franzen, P. E. Simms, A. F. Van Huis, K. E. Foreman, P. C. Kuo, G. N. Gupta, Characterization of uptake and internalization of exosomes by bladder cancer cells, *BioMed research international* 2014 (2014).
- [28] J. M. Tomczak, E. Weglarz-Tomczak, Estimating kinetic constants in the Michaelis-Menten model from one enzymatic assay using approximate Bayesian computation., *FEBS letters* 593 (2019) 2742–2750.
- [29] S. S. Andrews, D. Bray, Stochastic simulation of chemical reactions with spatial resolution and single molecule detail, *Physical biology* 1 (3) (2004) 137.
- [30] T. F. Coleman, Y. Li, An interior trust region approach for nonlinear minimization subject to bounds, *SIAM Journal on Optimization* 6 (2) (1996) 418–445.
- [31] J. A. D. Wattis, B. O’Malley, H. Blackburn, L. Pickersgill, J. Panovska, H. M. Byrne, K. G. Jackson, Mathematical model for low density lipoprotein (LDL) endocytosis by hepatocytes, *Bulletin of Mathematical Biology* 70 (8) (2008) 2303–2333.
- [32] H. J. Harwood, L. D. Pellarin, Kinetics of low-density lipoprotein receptor activity in Hep-G2 cells: derivation and validation of a Briggs–Haldane-based kinetic model for evaluating receptor-mediated endocytotic processes in which receptors recycle, *Biochem J.* 323 (1997) 649–659. doi:10.1042/bj3230649.